OPEN

First In-Human Results of Computed Tomography Angiography for Coronary Stent Assessment With a Spectral Photon Counting Computed Tomography

Sara Boccalini, MD, PhD,† Salim A. Si-Mohamed, MD, PhD,*† Hugo Lacombe, MsC,* Adja Diaw, MsC,* Mohammad Varasteh, PhD,* Pierre-Antoine Rodesch, PhD,* Marjorie Villien, PhD,‡ Monica Sigovan, PhD,* Riham Dessouky, MD, PhD,§ Philippe Coulon, PhD,‡ Yoad Yagil, PhD,|| Elias Lahoud, PhD,|| Klaus Erhard, PhD,¶ Gilles Rioufol, MD, PhD,# Gerard Finet, MD, PhD,# Eric Bonnefoy-Cudraz, MD, PhD,# Cyrille Bergerot, MD,# Loic Boussel, MD, PhD,*† and Philippe C. Douek, MD, PhD*†*

Objectives: The aim of this study is to compare the image quality of in vivo coronary stents between an energy integrating detectors dual-layer computed tomography (EID-DLCT) and a clinical prototype of spectral photon counting computed tomography (SPCCT).

Materials and Methods: In January to June 2021, consecutive patients with coronary stents were prospectively enrolled to undergo a coronary computed tomography (CT) with an EID-DLCT (IQon, Philips) and an SPCCT (Philips). The study was approved by the local ethical committee and patients signed an informed consent. A retrospectively electrocardiogram-gated acquisition was performed with optimized matching parameters on the 2 scanners (EID-DLCT: collimation, 64 × 0.625 mm; kVp, 120, automatic exposure control with target current at 255 mAs; rotation time, 0.27 seconds; SPCCT: collimation, 64 × 0.275 mm; kVp, 120; mAs, 255; rotation time, 0.33 seconds). The injection protocol was the same on both scanners: 65 to 75 mL of Iomeron (Bracco) at 5 mL/s. Images were reconstructed with slice thickness of 0.67 mm, 512 matrix, XCB (Xres cardiac standard) and XCD (Xres cardiac detailed) kernel, iDose 3 for EID-DLCT and 0.25-mm slice thickness, 1024 matrix, Detailed 2 and Sharp kernel, and iDose 6 for SPCCT. Two experienced observers measured the proximal and distal external and internal diameters of the stents to quantify blooming artifacts. Regions of interest were drawn in the lumen of the stent and of the upstream coronary artery. The difference (Δ S-C) between the respective attenuation values was calculated as a quantification of stent-induced artifacts on intrastent image quality. For subjective image quality, 3 experienced observers graded with a 4-point scale the image quality of different parameters: coronary wall before the stent, stent lumen, stent structure, calcifications surrounding the stent, and beam-hardening artifacts.

Results: Eight patients (age, 68 years [interquartile range, 8]; all men; body mass index, 26.2 kg/m^2 [interquartile range, 4.2]) with 16 stents were scanned. Five stents were not evaluable owing to motion artifacts on the SPCCT. Of the remaining, all were drug eluting stents, of which 6 were platinum-chromium, 3 were cobalt-platinum-iridium, and 1 was stainless steel. For 1 stent, no information could be retrieved. Radiation dose was lower with the SPCCT (fixed CT dose index of 25.7 mGy for SPCCT vs median CT dose index of 35.7 [IQ = 13.6] mGy; $P = 0.02$). For 1 stent, the internal diameter was not assessable on EID-DLCT. External diameters were smaller and internal diameters were larger with SPCCT (all $P < 0.05$). Consequently, blooming artifacts were reduced on SPCCT ($P < 0.05$). Whereas Hounsfield unit values within the coronary arteries on the 2 scanners were similar, the Δ S-C was lower for SPCCT-Sharp as compared with EID-DLCT-XCD and SPCCT-Detailed 2 ($P < 0.05$). The SPCCT received higher subjective scores than EID-DLCT for stent lumen, stent structure, surrounding calcifications and beam-hardening for both Detailed 2 and Sharp (all $P \leq 0.05$). The SPCCT-Sharp was judged better for stent structure and beam-hardening assessment as compared with SPCCT-Detailed 2.

Conclusion: Spectral photon counting CT demonstrated improved objective and subjective image quality as compared with EID-DLCT for the evaluation of coronary stents even with a reduced radiation dose.

Key Words: coronary stents, photon counting CT, coronary CT angiography, image quality

(*Invest Radiol* 2022;57: 212–221)

Stent assessment remains one of the biggest challenges of coronary computed tomography angiography (CCTA). Consequently, although CCTA is routinely integrated in the workflow of patients with stable chest pain and its role is currently under discussion for patients with acute chest pain without ST elevation, its implementation in clinical practice for stent assessment is still debated, especially for stents with diameters smaller than 3 mm.[1,2]

Undeniably, different types of artifacts due to the metallic structure of the stents, namely, blooming and beam-hardening streak artifacts, are well-known limitations for the assessment of coronary stents ever since submillimetric spatial resolution made it feasible.[3] Although developments in computed tomography (CT) technology resulted in improved visualization of stent lumen,[4] even CT scanners with 320 rows of energy integrating detectors (EIDs) yield a positive predictive value of only 46%[5] for the detection of intrastent restenosis (ISR). The most common complication after stent placement, ISR should be promptly detected as it necessitates a reintervention in 6% of cases.[6,7]

Received for publication July 22, 2021; and accepted for publication, after revision, August 18, 2021.

From the *University Lyon, INSA-Lyon, University Claude Bernard Lyon 1, UJM-Saint Etienne, CNRS, Inserm, Villeurbanne, France; †Department of Cardiovascular and Thoracic Radiology, Louis Pradel Hospital, Hospices Civils de Lyon, Bron, France; ‡Philips Healthcare, Suresnes, France; §Department of Radiology, Faculty of Medicine, Zagazig University, Zagazig, Egypt; ||Philips Healthcare, Haifa, Israel; ¶Philips Research, Hamburg, Germany; and #Department of Cardiology, Louis Pradel Hospital, Hospices Civils de Lyon, Bron, France.

Conflicts of interest and sources of funding: European Union Horizon 2020 research and innovation program under grant agreement no. 668142.

Sara Boccalini and Salim A. Si-Mohamed share first authorship, with equal contribution.

Correspondence to: Sara Boccalini, MD, PhD, Department of Cardiovascular Radiology, Hopital Pradel, 59 Boulevard Pinel, 69500 Bron, France. E-mail: sara.boccalini@yahoo.com; sara.boccalini@chu-lyon.fr.

Supplemental digital contents are available for this article. Direct URL citations appear in the printed text and are provided in the HTML and PDF versions of this article on the journal's Web site (www.investigativeradiology.com).

Copyright © 2021 The Author(s). Published by Wolters Kluwer Health, Inc. This is an open-access article distributed under the terms of the Creative Commons Attribution-Non Commercial-No Derivatives License 4.0 (CCBY-NC-ND), where it is permissible to download and share the work provided it is properly cited. The work cannot be changed in any way or used commercially without permission from the journal.

ISSN: 0020-9996/22/5704–0212
DOI: 10.1097/RLI.0000000000000835

In the last years, new CT scanners featuring photon counting detectors (PCDs) have emerged thanks to their innovative characteristics. Made of different materials, such as cadmium-zinc-telluride, allowing direct conversion of photons into energy, PCDs capture more accurately the spectrum of attenuations, especially at low energies. Smaller in size and relieved of other interposed components as opposed to EID, directly converting PCDs allow for improved spatial resolution and dose efficiency as well as noise and artifact reduction.[8,9] Recently tested and confirmed on the first human lung and vascular scans,[10–12] features of CT systems with PCDs (PCCTs) are likely to result also in improved image quality of coronary stents.

Indeed, a few preliminary studies with a PCCT scanner and a spectral PCCT (SPCCT), which allows for spectral and k-edge imaging,[11,13,14] confirmed the feasibility as well as the amelioration of image quality of coronary stents scanned in vitro and in animals.[15–19] Notwithstanding these promising results, to the best of our knowledge, there are so far no data regarding the assessment of coronary stents in humans.

Therefore, the aim of our study was to compare objective and subjective image quality of in vivo coronary stents as assessed with CCTA imaging on a commercially available EID dual-layer CT scanner (EID-DLCT) and a clinical SPCCT prototype.

MATERIALS AND METHODS

Study Population

This was a prospective observational monocentric study carried out in a tertiary care university hospital. The study was approved by the local institutional review board (N ID-RCB: 2019-A02945-52) and all patients signed an informed consent. In January to June 2021, 8 consecutive patients with coronary stents were prospectively enrolled to undergo 2 coronary CT scans with both a commercially available EID-DLCT (IQon, Philips, Haifa, Israel) and an SPCCT (Philips, Haifa, Israel). The scans were performed with a maximum delay of 3 days in between. Clinical indications for the coronary CT scans were stent or coronary artery disease assessment in patients with recurrent chest pain and/or a specific electrocardiographic anomaly and stent deployment assessment after difficult procedures.

SPCCT System

The SPCCT was a clinical prototype with a large field of view (FOV; of 500 mm in-plane) featuring energy-sensitive PCDs of 2-mm-thick cadmium-zinc-telluride, bonded to Philips' proprietary ChromAIX2 application-specific integrated circuit.[20] Pixel dimensions at the isocenter are 270 × 270 μm^2. This system allowed the configuration of 5 controllable energy thresholds that were set at 30, 51, 62, 72, and 81 keV for optimized image quality on iodine enhanced images.

EID-DLCT and SPCCT Acquisition Parameters

An acquisition with retrospective electrocardiogram (ECG) gating was performed with optimized matching parameters on the 2 scanners (EID-DLCT: collimation, 64 × 0.625 mm; rotation time, 0.27 seconds; pitch 0.16; SPCCT: collimation, 64 × 0.275 mm; rotation time, 0.33 seconds; pitch 0.32). For both systems, the tube voltage was set at 120 kVp with a current fixed at 255 mAs for SPCCT, whereas for EID-DLCT, automatic exposure control was used with a DoseRight index of 28 corresponding to a target current at 255 mAs for average adult patient size with water equivalent diameter of 29 cm.

Injection Protocol

The injection protocol was the same on the 2 scanners: 65 or 75 mL of Iomeron 400 mg/mL (Bracco, Milan, Italy) at 5 mL/s, depending on the patient's weight (< or >80 kg), followed by 20 mL at 4 mL/s of saline. The timing of the acquisition after injection was established differently on the 2 scanners. For EID-DLCT, bolus tracking with a region of interest (ROI) placed in the descending aorta and a threshold of 110 HU was used. For SPCCT, a bolus test was performed with 20 mL of contrast media at 5 mL/s, followed by 20 mL of saline solution at 4 mL/s to calculate the appropriate delay.

Unless contraindicated, a sublingual spray of nitroglycerin (Natispray; Teofarma SRL, Italy) was administered to all patients and an intravenous injection of β-blockers (esmolol chlorohydrate, Esmocard; Orpha Devel Handels Vertriebs GMBH, Austria) was added if the patient's heart rate was above 70 bpm.

Image Reconstruction

Preliminarily, images from different phases were reconstructed on at least 3 different phases of the cardiac cycle (0%, 40%, and 78%) to define which one had the least motion artifacts and thus allowed the best visualization for each stent.

Once the best phase/s were identified, the images for the final analysis were reconstructed based on manufacturers' suggestions and a preliminary selection among available parameters by 3 experienced cardiovascular radiologists (PD, SB and SSM, with 30, 7, and 7 years of experience, respectively).

The selected parameters were 0.67 mm with 0.4 mm increment, 512 matrix, XCB (Xres cardiac standard) and XCD (Xres cardiac detailed) kernel for EID-DLCT and 0.25 mm slice thickness, 0.25 mm increment, 1024 matrix, and Detailed 2 and Sharp kernel for SPCCT. Hybrid iterative reconstruction, iDose^4 for the EID-DLCT and an adapted iDose-like algorithm for SPCCT, was used for both CT systems with a level of 3 for EID-DLCT and of 6 for SPCCT.

Information on acquisition and reconstruction parameters for the 2 systems can be found in Table 1.

Preliminary Image Quality Assessment for Stent Inclusion

On the selected cardiac phases, the presence of motion artifacts was further analyzed and each stent was classified as evaluable or not. Stents for which only 1 portion was deemed assessable were classified as evaluable if this part was of sufficient length (at least 1 cm length) for objective and subjective evaluation. In case of segments of the same stent demonstrating different characteristics (eg, emerging branches

TABLE 1. EID-DLCT and SPCCT Acquisition and Reconstruction Parameters

	EID-DLCT	SPCCT
Acquisition parameters		
Collimation, mm	64 × 0.625	64 × 0.275
Tube voltage, kV	120	120
Tube current, mAs	Reference 255	255
Dose modulation	DoseRight	None
Rotation time, s	0.27	0.33
Pitch	0.16	0.32
Reconstruction parameters		
FOV, mm	220	220
Matrix, pixels	512 × 512	1024 × 1024
Slice thickness, mm	0.67	0.25
Increment, mm	0.34	0.25
Voxel size, mm	0.625(z) × 0.43(x) × 0.43(y)	0.25(z) × 0.21(x) × 0.21(y)
Kernel	XCB and XCD	Detailed 2 and Sharp
Iterative reconstruction	iDose 3	iDose 6

EID-DLCT indicates energy integrating detectors dual-layer computed tomography; FOV, field of view; SPCCT, spectral photon counting computed tomography; XCB, Xres cardiac standard; XCD, Xres cardiac detailed.

© 2021 The Author(s). Published by Wolters Kluwer Health, Inc.

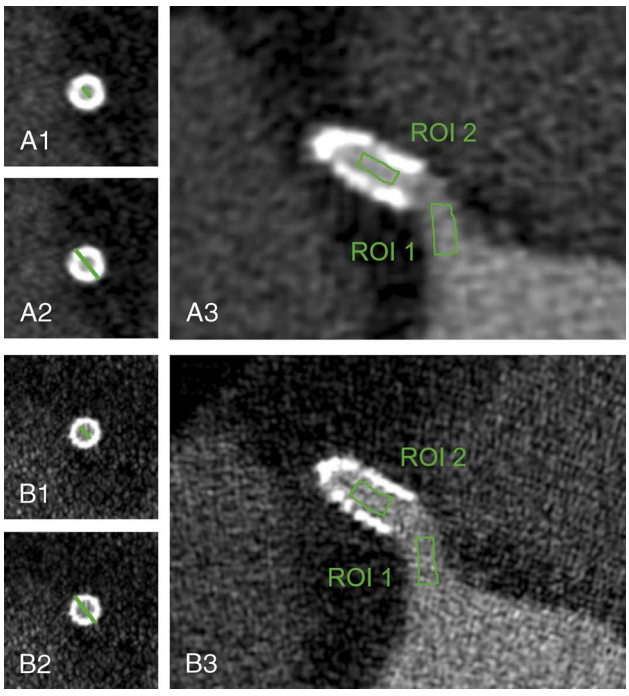

FIGURE 1. Panels A1-A2 and B1-B2 show how internal (A1 and B1) and external (A2 and B2) stent diameters have been measured on EID-DLCT (A) and SPCCT (B). Panels A3 and B3 illustrate how the free-hand ROIs have been drawn on EID-DLCT (A) and SPCCT (B) inside the coronary artery upstream the stent (ROI 1) and inside the lumen of the stent (ROI 2). Images are displayed in the window level and window width used for objective analysis, as defined in the methodology.

with clear caliber discontinuation on the main stent, stent-in-stent, etc), different segments were analyzed separately for both subjective and objective analysis but diameters were measured at only 1 location per segment.

Analysis of Stent Image Quality

For each stent, both objective and subjective analyses were performed on a commercially available multimodality multiplanar workstation (IntelliSpace Portal, Philips, Best, the Netherlands).

Stent diameters were independently measured by 2 radiologists (SB and SSM, with 7 and 7 years' experience in cardiovascular imaging, respectively). Further data for objective image quality were collected upon definition of correct measurement planes and ROIs by the 2 radiologists blinded to image type.

Subjective analysis was independently performed by 3 radiologists (PD, SB, and SSM with 30, 7, and 7 years' experience in cardiovascular imaging, respectively).

Objective Image Quality

Stent structure (stent diameters as well as derived blooming artifacts and struts thickness) and lumen (attenuation inside and outside of the stent and its difference) were objectively evaluated.

For these analyses, manual double oblique multiplanar reconstructions of each stent were performed to obtain matching long axis and cross-axial views of the stent for the EID-DLCT-XCD kernel and the 2 SPCCT kernels (Detailed 2 and Sharp). The window level value was equal to the density of an ROI measurement in the aorta for each reconstruction. The window width was then set to a value obtained by multiplying the window level value for 2.5.[17]

Stent Structure

Linear measurements of the maximal internal and external diameter of the proximal and distal part of the stent were performed on cross-

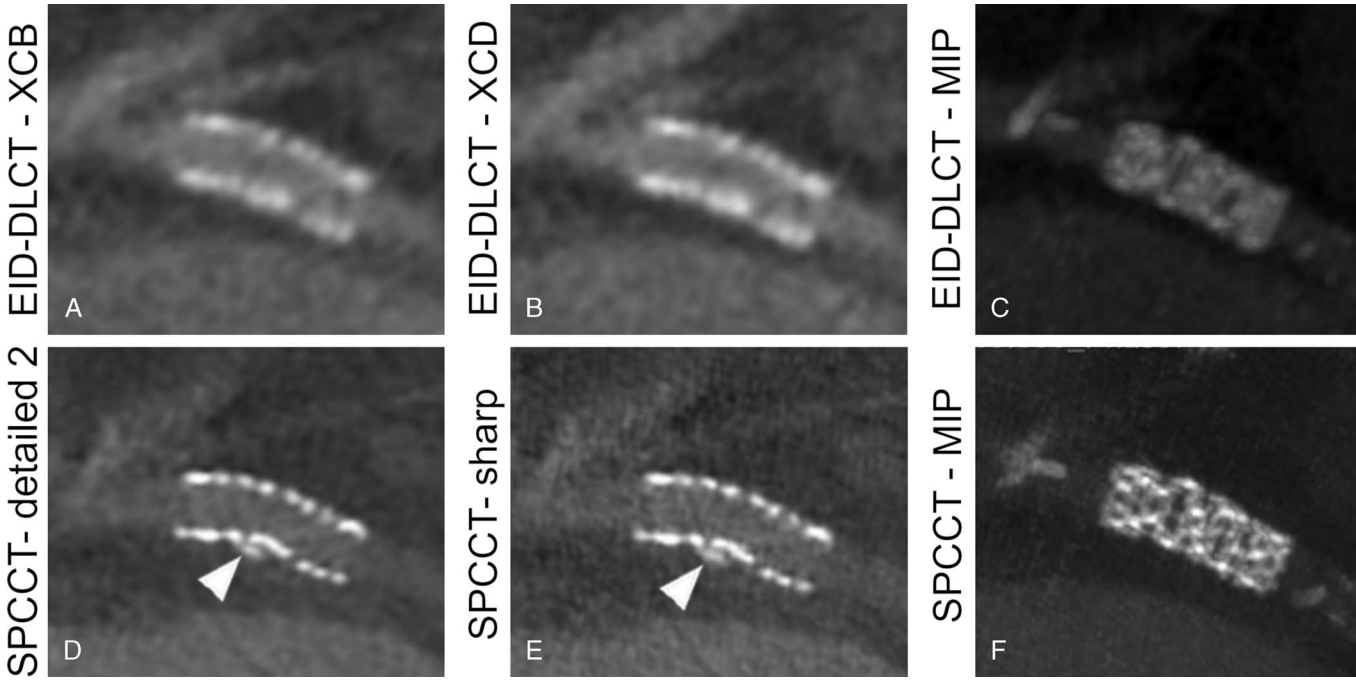

FIGURE 2. A synergy 3.5 × 12 mm stent placed in the proximal circumflex artery of a 72-year-old man depicted with EID-DLCT (A, B, and C) and SPCCT (D, E, and F). The structure of the stent is difficult to assess on both EID-DLCT multiplanar images reconstructed with both kernels (A: EID-DLCT-XCB; B: EID-DLCT-XCD) as well as on the EID-DLCT maximum intensity projection (MIP) (C) image while being clearly defined on SPCCT multiplanar (D: SPCCT-Detailed 2; E: SPCCT-Sharp) and MIP (F) images. The EID-DLCT also failed to depict a small calcification adjacent of the stent, nicely shown by SPCCT (D and E: arrowheads).

© 2021 The Author(s). Published by Wolters Kluwer Health, Inc.

axial reconstructions by 2 radiologists (SB and SSM) (Fig. 1). Measurements were performed in areas of the stent without detectable adjacent calcifications. Based on mean measurements (average of proximal and distal), an estimation of the blooming artifacts was calculated according to the following formula[21]:

$$\text{Blooming} = \frac{\text{Measured external stent diameter} - \text{Measured internal stent diameter}}{\text{Measured external stent diameter}} \times 100\%$$

The thickness of the stent struts as calculated on CT images was compared with the nominal values provided by the manufacturers. For CT, strut thickness was obtained as follows: (mean external stent diameter-mean internal stent diameter) / 2.

Stent Lumen

Thereafter, on long axis views, manually drawn ROIs of at least 2 mm^2 were drawn in the lumen of the coronary artery just before the stent (ROI1) and inside the circulating lumen of the stent (ROI2) (Fig. 1). For each ROI, average attenuation values in Hounsfield unit (HU) and standard deviation were noted. Standard deviation was considered as a measure of noise. The difference between the lumen attenuation inside and before the stent was calculated (Δ S-C = ROI2 HU – ROI1 HU)[17] as a measure of the effect of stent-induced artifacts on intrastent lumen image quality.

Subjective Image Quality

Subjective image quality was assessed for the visualization of the stent lumen, the coronary wall just upstream and downstream the stent extremities, the stent structure, the calcifications apposed to the stent structure, and beam-hardening artifacts. For each of these parameters a 4-point Likert scale was used as detailed below.

For the lumen of the stent:

(1) Unacceptable, nondiagnostic image quality; (2) poor, limited diagnostic value; (3) good, diagnostic image quality; or (4) excellent, optimal diagnostic image quality.

For the coronary artery wall next to the stent extremities:

(1) Unacceptable, nondiagnostic image quality, the coronary wall is not visible because of stent artifacts; (2) poor, limited diagnostic value, stent artifacts interfere with the assessment of the coronary wall; (3) good, diagnostic image quality, the coronary wall and the stent extremity are well visible; or (4) excellent, optimal diagnostic image quality, the coronary wall and its relationship with the stent extremity are perfectly visible without artifacts.

For the structure of the stent:

(1) Unacceptable, nondiagnostic image quality of the stent structure, not assessable because of severe artifacts or excessive noise; (2) poor, image quality of the stent structure with limited diagnostic value, the structure is visible but difficult to analyze because of moderate artifacts or noise; (3) good, diagnostic image quality of the stent structure, possible to diagnose/exclude stent structure abnormalities and to distinguish struts with minor artifacts or noise; or (4) excellent, excellent image quality of the aortic wall, possible to diagnose/exclude coronary wall abnormalities and to distinguish struts without artifacts or noise.

For the outer calcifications:

(1) Unacceptable, nondiagnostic image quality of the coronary wall, calcifications not assessable because of severe artifacts or excessive noise; (2) poor, image quality of the coronary wall with limited diagnostic value, calcifications are visible but difficult to differentiate because of moderate artifacts or noise; (3) good, diagnostic image quality of the coronary wall, possible to diagnose/exclude coronary wall abnormalities with minor artifacts or noise; or (4) excellent, excellent image quality of the aortic wall, possible to diagnose/exclude coronary wall abnormalities without artifacts or noise.

For beam-hardening artifacts:

(1) Unacceptable artifacts, nondiagnostic image quality of tissues around the stent; (2) marked artifacts, limited diagnostic value on tissues around the stent and acceptable image quality inside the stent; (3) moderate artifacts, diagnostic image quality inside and outside the stent; or (4) no artifact, optimal diagnostic image quality.

For the assessment of the coronary wall upstream and downstream the stent extremities, the 2 kernels for each CT scanner were judged (Fig. 2). For all other parameters, the EID-DLCT-XCD and both SPCCT kernels were scored.

Observers were free to set windowing and zoom parameters according to personal preferences. Maximum intensity projections could be used to assess the stent structure at the discretion of the observers.

Statistical Analysis

Statistical analysis was performed with SPSS, version 21 (IBM, Armonk, NY).

Continuous variables are presented as average ± standard deviation or median (interquartile range [IQ]) as appropriate. Normal distribution

TABLE 2. Patients Characteristics and Stent Information

Patients					
Sex			All men		
Height, cm			172 (8)		
Weight, kg			81 (12.5)		
BMI, kg/m^2			26.17 (4.16)		
CT acquisitions	**EID-DLCT**	**SPCCT**	***P***		
Heart frequency, bpm	60 (13.5)	60 (12.5)	0.37		
$CTDI_{vol}$, mGy	35.7 (13.6)	25.7	0.02		
DLP, mGy*cm	698 (242)	476	0.02		
Stents					
Name	**Synergy**	**Resolute Onyx**	**BiOSS LIM**	**Unknown**	**Total**
N	6	3	1	1	11
Metallic structure	Platinum-chromium	Cobalt-platinum-iridium	Stainless steel		
Drug	Everolimus	Zotarolimus	Sirolimus		
Localization					
Prox LAD	3	1	–	1	5
Mid LAD	–	–	1	–	1
Dist LAD	–	2	–	–	2
Diagonal	1	–	–	–	1
Prox LCX	1	–	–	–	1
RCA	1	–	–	–	1
Dimensions					
Diameter					
<3 mm	1	2	–		3
>3 mm	5	1	1	–	7
Length					
<15 mm	2	1	–		3
>15 mm	4	2	1		7

Continuous variables are indicated as median (interquartile range).

BMI indicates body mass index; $CTDI_{vol}$, computed tomography dose index; DLP, dose length product; EID-DLCT indicates energy integrating detectors dual-layer computed tomography; LAD, left anterior descending; LCX, left circumflex artery; RCA, right coronary artery; SPCCT, spectral photon counting computed tomography.

© 2021 The Author(s). Published by Wolters Kluwer Health, Inc.

TABLE 3. Comparison of Stent Diameters and Blooming Artifacts Between EID-DLCT and SPCCT With Different Kernels

		EID-DLCT	SPCCT		XCD vs Sharp	Detailed 2 vs Sharp
		XCD	Detailed 2	Sharp	*P*	*P*
Proximal diameter						
Internal, mm	Obs 1	1.30 (1.15)	1.90 (1.05)	2.00 (0.95)	**0.002**	**0.04**
	Obs 2	1.55 (2.35)	2.30 (0.95)	2.3 (1.00)	**0.007**	0.76
External, mm	Obs 1	5.0 (1.10)	4.50 (1.25)	4.40 (1.35)	**0.011**	1.00
	Obs 2	4.45 (1.03)	4.10 (0.85)	4.10 (0.95)	**0.010**	0.71
Distal diameter						
Internal, mm	Obs 1	1.45 (1.30)	2.00 (0.70)	1.90 (0.90)	**0.005**	0.23
	Obs 2	1.85 (2.35)	2.10 (1.10)	2.20 (1.10)	**0.007**	0.48
External, mm	Obs 1	4.30 (1.00)	4.10 (1.60)	3.90 (1.20)	**0.007**	0.07
	Obs 2	4.30 (1.33)	3.80 (1.30)	3.80 (1.60)	**0.007**	0.25
Blooming, %						
	Obs 1	71.26 (27.23)	57.41 (13.49)	53.38 (11.90)	**0.002**	**0.012**
	Obs 2	62.96 (43.90)	41.49 (11.33)	39.36 (11.69)	**0.003**	0.42

Continuous variables are presented as median (interquartile range). Data in bold indicate significant values.

EID-DLCT indicates energy integrating detectors dual-layer computed tomography; SPCCT, spectral photon counting computed tomography; XCD, Xres cardiac detailed.

was verified with Shapiro test and Q-Q plots. Wilcoxon signed-rank test was used to test differences between objective measurements performed on the 2 comparable kernels of the 2 systems and on the 2 SPCCT kernels. These comparisons were performed separately without any further correction in this exploratory study where the interest was focused on the pairwise comparison of these 2 specific and different scenarios. For subjective image quality assessment, the Friedman test with Dunn-Bonferroni correction was used. A P value of <0.05 was considered statistically significant.

RESULTS

Patients, Stents, and Acquisitions

Eight patients (age, 68 years [IQ, 8]; all men; body mass index, 26.2 kg/m^2 [IQ, 4.2]) with 16 stents were scanned.

Five stents were not assessable because of motion artifacts on the SPCCT (2 stents on the right coronary artery, 2 on the left circumflex artery, and 1 in the left anterior descending), leaving 7 patients with

TABLE 4. Comparison of Coronary Artery and Stent Lumen ROI Data (Surface, HU, and Noise) Between the 2 Systems and Different SPCCT Kernels

		EID-DLCT	SPCCT		XCD vs Sharp	Detailed 2 vs Sharp
		XCD	Detailed 2	Sharp	*P*	*P*
Coronary artery						
Surface, mm^2	Obs 1	12.0 (5.4)	10.8 (6.2)	11.0 (1.9)	0.63	0.13
	Obs 2	5.5 (1.3)	6.4 (1.8)	6.4 (1.8)	0.15	0.32
Density, HU	Obs 1	510 (194)	439.3 (243.8)	446.2 (236.1)	0.63	0.46
	Obs 2	521 (161)	450 (245)	455 (247)	0.75	0.11
SD	Obs 1	65.3 (17.7)	60.6 (17.4)	135.2 (65.5)	**0.002**	**0.001**
	Obs 2	56.9 (2.3)	49 (6.5)	157 (23)	**0.003**	**0.001**
Stent lumen						
Surface, mm^2	Obs 1	3.2 (2.1)	3.2 (3.2)	4.3 (2.6)	0.24	0.65
	Obs 2	6.3 (4.5)	2.2 (2.2)	2.2 (2.1)	**0.002**	0.53
HU, HU	Obs 1	629 (449)	519 (321)	512 (311)	**0.01**	**0.04**
	Obs 2	608 (723)	535 (303)	520 (309)	**0.008**	**0.008**
SD	Obs 1	56.6 (26.0)	70.4 (50.7)	122.5 (75.3)	**0.002**	**0.004**
	Obs 2	88 (62.9)	96.1 (41.8)	98.9 (55.4)	0.24	**0.028**
Δ S-C*						
	Obs 1	148 (304)	109 (90)	84 (61)	**0.04**	**0.019**
	Obs 2	210 (377)	124 (92)	107 (106)	**0.023**	**0.005**

Continuous variables are presented as median (interquartile range). Data in bold indicate significant values.

* Medians of the absolute values of the Δ S-Cs.

EID-DLCT indicates energy integrating detectors dual-layer computed tomography; HU, Hounsfield unit; ROI, region of interest; SPCCT, spectral photon counting computed tomography; XCD, Xres cardiac detailed.

© 2021 The Author(s). Published by Wolters Kluwer Health, Inc.

11 stents (corresponding to 13 segments of interest) available for further analysis. Of the included stents, 6 were drug eluting stents (DESs) with a metallic structure composed of platinum-chromium (Synergy, Boston Scientific, Marlborough, MA), 3 of cobalt-platinum-iridium (Resolute Onyx, Medtronic, Minneapolis, MN), and 1 of stainless steel (BiOSS LIM, Balton, Warsaw, Poland). The 11th stent was also a DES, but no further information was retrievable. Of the 11 stents, 8 were placed in the left anterior descending, 1 on the diagonal, 1 on the left circumflex artery, and 1 on the right coronary artery.

For 1 stent segment, the EID-DLCT-XCD reconstruction at the appropriate phase of the cardiac cycle was not available for analysis.

The patients' heart rate during the 2 examinations on the 2 scanners was similar: 60 (IQ, 13.5) for EID-DLCT and 60 (IQ, 12.5) for SPCCT ($P = 0.37$).

The per-patient dose delivered with the scans was lower with the SPCCT (with a fixed CT dose index of 25.7 mGy and dose length product of 475.7 mGy*cm) as compared with the EID-DLCT (median CT dose index of 35.7 [IQ, 13.6] mGy and dose length product of 698 [IQ, 242] mGy*cm) ($P = 0.02$).

Patient, stent, and acquisition characteristics are presented in Table 2.

Objective Image Quality

Stent Structure

Measures of stent diameters and blooming effect are reported in Table 3.

Measures of proximal and distal external stent diameters were significantly smaller for SPCCT as compared with EID-DLCT for both observers (all $P < 0.05$), whereas all internal diameters were larger with SPCCT (all $P < 0.05$). For 1 stent, internal diameters were not measurable on EID-DLCT because of the artifacts making the stent lumen indistinguishable. Only the proximal internal diameter as measured by 1 observer was different between the 2 kernels of SPCCT ($P = 0.04$).

Consequently, blooming artifacts were more pronounced on EID-DLCT than on SPCCT for both observers, with, for example, values of 71% on EID-DLCT-XCD and 53% on SPCCT-Sharp. Only for 1 observer was SPCCT-Sharp blooming lower than for SPCCT-Detailed 2 ($P = 0.012$).

Nominal values of stent strut thickness as provided by manufacturers were 0.074 mm for the Synergy, 0.07 mm for the Bioss Lim, and 0.081 mm for the Resolute Onyx. Differences between stent struts thickness calculated on CT measurements compared with nominal

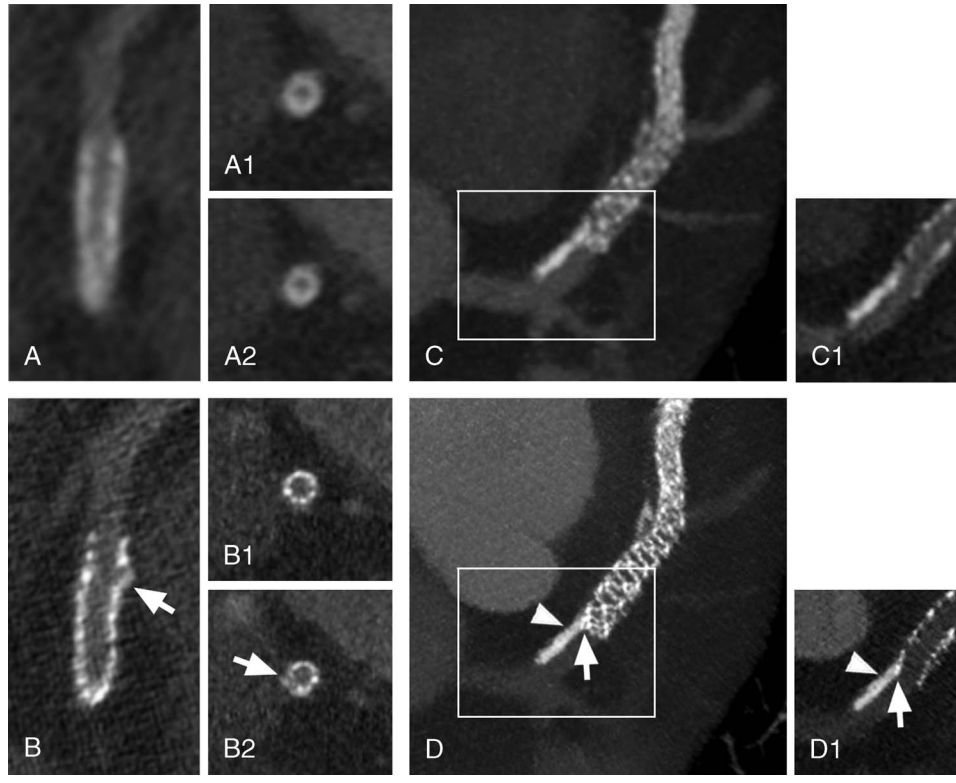

FIGURE 3. Stent extremities evaluation. Panels A (EID-DLCT-XCD) and B (SPCCT-Sharp) show a 3 × 30 mm Resolute Onyx stent of the proximal left anterior descending (LAD) in a 63-year-old patient. Long axis images of the proximal extremity of the stent are quite different between the 2 CT systems: whereas the outer border of the stent seems regular on EID-DLCT (A), an irregularity is clearly seen on SPCCT (B: arrow). Cross-axial images of the stent (at the proximal extremity of the stent (A1 and B1) and at the level of the irregularity (A2 and B2) showed a similarly homogeneous and blurry stent contour on EID-DLCT (A1 and A2). On the contrary, SPCCT nicely showed regular stent struts at the extremity (B1) and a hyperdense linear image protruding from the stent border (B2: arrow) at the level of the irregularity, suggesting a disrupted strut. Panels C (EID-DLCT-XCD) and D (SPCCT-Sharp) show the proximal extremity of a 3 × 48 mm Synergy stent of the proximal LAD in a 52-year-old patient. A maximum intensity projection (MIP) (C) reconstruction of the EID-DLCT showed a calcification of the upstream coronary wall, but its relationship with the stent was difficult to assess even when looking more closely on a multiplanar reconstruction (C1, corresponding to the white box on C). SPCCT images (D: MIP; D1: multiplanar reconstruction corresponding to the white box on D) not only allowed to depict sharp images of the stent struts and the coronary calcification (arrowheads) but also clearly showed that the proximal extremity of the stent was dislocated and pushed towards the center of the artery by the calcification (arrows).

© 2021 The Author(s). Published by Wolters Kluwer Health, Inc.

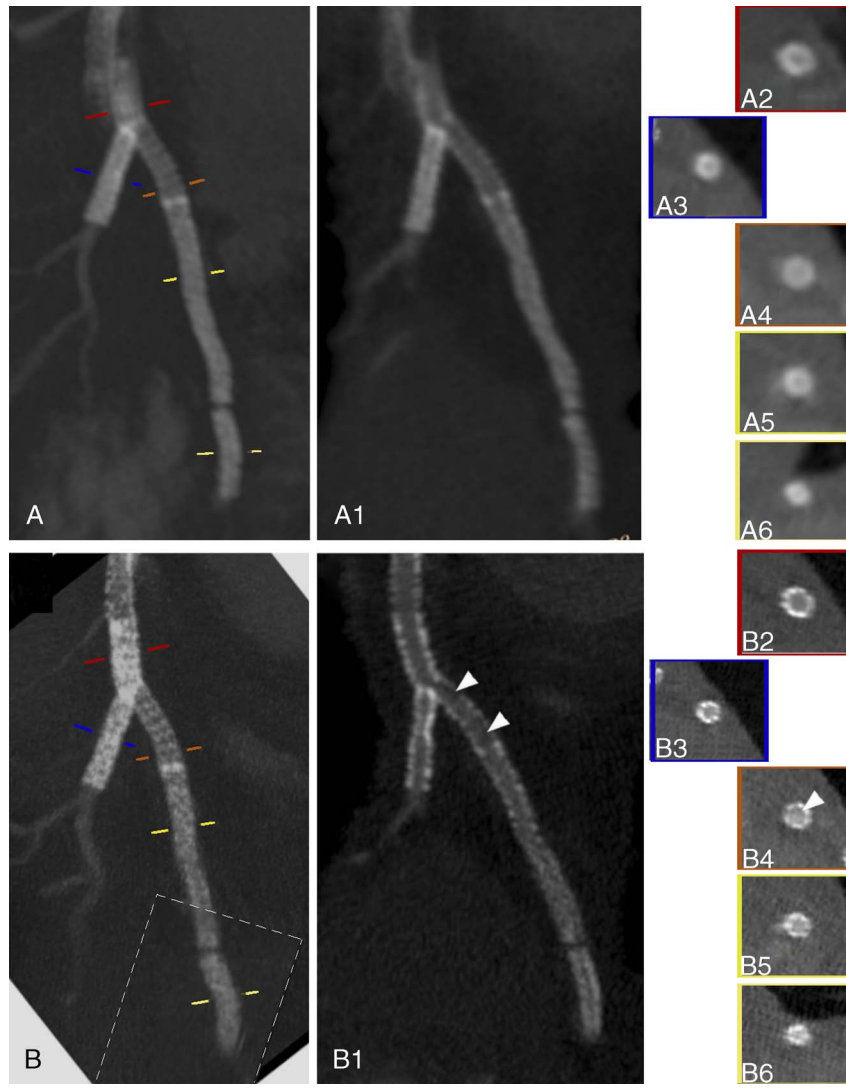

FIGURE 4. EID-DLCT-XCD (A) and SPCCT-Sharp (B) curved planar reformation with (A and B) and without (A1 and B1) maximum intensity projection and cross-sectional images (A2-A6 and B2-B6) show the 4 stents of a 70-year-old man: a 3.5 × 24 mm Bioss Lim of the proximal left anterior descending (LAD) (orange line on A and B, A4 and B4), 2 Resolute Onyx stents of 2.5 × 30 mm (yellow line on A and B, A5 and B5), and 2.25 × 12 mm (light yellow line on A and B, A6 and B6) of the distal LAD as well as a 3 × 38 mm Synergy stent (blue line on A and B, A3 and B3) of the first diagonal branch. The latest has been deployed with a Y configuration, thus realizing a few millimeters of stent-in-stent (red line on A and B, A2 and B2). Even disregarding the proximal part of the first stent of the LAD that showed marked motion artifacts, the EID-DLCT system does not allow correct visualization of any of the stent lumina. On the contrary, SPCCT allows visualization of the stent struts and their lumina, suggesting the presence of restenosis on the first Resolute Onyx (arrowheads). The dotted-line box on B shows where an image reconstructed from a different phase of the cardiac cycle has been pasted for display.

values are displayed in Figure 1, Supplemental Material, http://links.lww.com/RLI/A654. Although there seemed to be differences between different types of stents, no further analysis was performed considering the low number of stents per type.

Stent Lumen

Data extracted from ROIs placed in the coronary artery just upstream the stent and in the stent lumen as well as the Δ S-C are reported in Table 4.

On the 2 different acquisitions performed with the 2 systems, coronary arteries showed similar attenuation on EID-DLCT and SPCCT ($P = 0.63$ and $P = 0.75$ for the 2 observers, respectively). No difference in attenuation in the coronary artery was found between different kernels of SPCCT ($P = 0.46$ and $P = 0.11$).

Intrastent attenuation values were lower for SPCCT ($P < 0.05$). Lower attenuation (difference of 7 HU, $P = 0.04$, and 15 HU, $P = 0.008$, for the 2 observers) was also recorded on SPCCT-Sharp as compared with SPCCT-Detailed 2. Consequently, the intralumen artifacts induced by the stent structure were less pronounced on SPCCT as highlighted by the Δ S-C values that were 44% to 49% lower on SPCCT-Sharp as compared with EID-DLCT-XCD (both $P < 0.05$) and 14% to 23% lower on SPCCT-Sharp compared with SPCCT-Detailed 2 (both $P < 0.05$).

The SPCCT-Sharp kernel yielded more noise in the coronary arteries and in the stent lumen as compared with both EID-DLCT-XCD and SPCCT-Detailed 2 (all $P < 0.05$).

© 2021 The Author(s). Published by Wolters Kluwer Health, Inc.

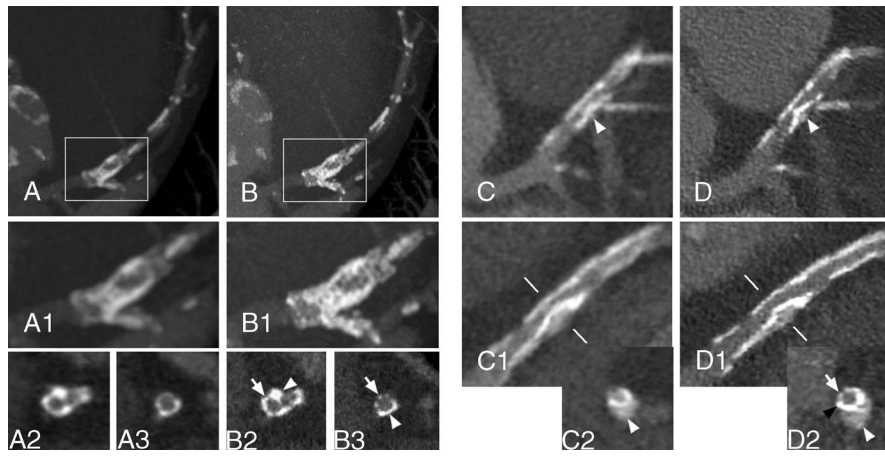

FIGURE 5. Stent calcifications. Panels A (EID-DLCT-XCD) and B (SPCCT-Sharp) show a DES of the left anterior descending (LAD), extending over the origin of the diagonal, of a 69-year-old man deployed in 2007. On maximum intensity projection (MIP) (A and A1; A1 corresponds to the white box in A) and cross-axial (A2 and A3 at the level of the origin of the diagonal and a bit further downstream, respectively) reconstructions of the EID-DLCT, some hyperdense images on the walls of the coronary images could represent either calcifications or struts since the stent structure is undistinguishable. Corresponding images on SPCCT (MIP in B and B1; B1 corresponds to the white box in B; cross-sectional in B2 and B3) nicely show the stent struts (arrows) encrusted with calcifications (arrowheads). In panels C (EID-DLCT-XCD) and D (SPCCT-Sharp), a 3.5 × 12 mm Synergy stent of the LAD, extending over the origin of the diagonal, implanted 5 months before the CT scans. The stent had been placed over a rather voluminous calcification (white arrowheads) that is deforming the stent lumen as it is visible on EID-DLCT (C, C1, and C2; C2: cross-axial image at the level of the white lines on C1) as well as on corresponding SPCCT images (D, D1, and D2). The lumen of the stent is hard to assess on EID-DLCT, whereas it is clearly reduced in caliber but patent on SPCCT. Furthermore, on the SPCCT cross-axial image (D2), the stent struts are nicely visible on 1 side (arrow), whereas on the other side, the calcification has 1 peripheral less dense component (white arrowhead) and a denser layer closer to the stent (black arrow).

Subjective Image Quality

Examples of stent extremities and adjacent coronary artery wall, stent structure and lumen assessment as well as calcifications imaged with EID-DLCT and SPCCT are provided in Figures 3, 4, and 5.

Mean scores of the 3 observers for the 5 assessed parameters are reported in Figure 6.

Image quality scores were significantly better for all parameters for SPCCT. This was true when comparing EID-DLCT-XCB versus SPCCT-Detailed 2 for coronary wall assessment as well as EID-DLCT-XCD versus SPCCT-Detailed 2 and EID-DLCT-XCD versus SPCCT-Sharp for all parameters (all $P < 0.05$). The only exception was found for beam hardening where EID-DLCT-XCD and SPCCT-Detailed 2 had similar values as highlighted by the post hoc test ($P = 0.19$).

The percentage of scores higher than 3, indicating good diagnostic image quality, for EID-DLCT-XCD, SPCCT-Detailed 2, and SPCCT-Sharp were 28% versus 85% versus 90% for intralumen, 36% versus 89% versus 96% for coronary wall, 28% versus 90% versus 90% for stent structure, 28% versus 97% versus 97% for calcifications, and 33% versus 69% versus 79% for beam-hardening.

Image quality was significantly better with SPCCT-Sharp as compared with SPCCT-Detailed 2 only for stent structure (4 [0.83] vs 3.67 [0.33]) and beam-hardening (3.33 [0.67] vs 2.67 [0.67]) assessment ($P < 0.05$). The image quality of calcifications was not significantly different between the 2 SPCCT reconstructions but was judged excellent with SPCCT-Sharp (4 [0.17]) and almost excellent with SPCCT-Detailed 2 (3.67 [0.33]).

DISCUSSION

Compared with a commercial EID-DLCT, SPCCT demonstrated improved image quality for in vivo assessment of coronary artery stents. With the Sharp kernel, SPCCT images demonstrated decreased Δ attenuation between the stent lumen and the upstream coronary lumen, reflecting a reduction in intrastent artifacts. External stent diameters were larger and internal diameters were lower on EID-DLCT, translating in

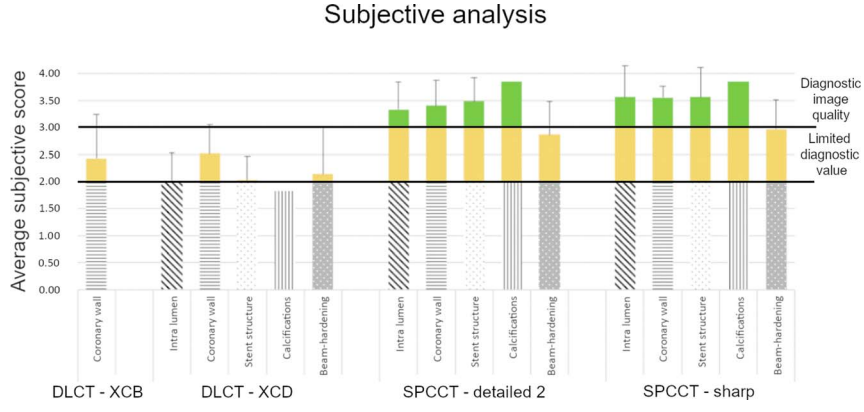

FIGURE 6. Average subjective scores.

© 2021 The Author(s). Published by Wolters Kluwer Health, Inc.

consistently more pronounced blooming artifacts on EID-DLCT. Subjective image quality scored higher for SPCCT for all parameters. The Sharp kernel showed some advantages over a less sharp kernel on SPCCT (Detailed 2), especially regarding artifact reduction and subjective stent structure assessment.

After its introduction in 1977, stent placement has been the mainstay treatment for coronary stenosis and one of the most commonly performed procedures in developed countries.[22] Although recent studies have challenged the benefit of stent treatment as compared with optimized medical treatment in patients with stable coronary artery disease,[23] invasive treatment remains the reference for unstable chest pain.[2] After stent treatment, neointimal hyperplasia is a common phenomenon leading to ISR in up to one third of patients.[22] Despite the introduction of first- and second-generation DES, ISR remains quite frequent, occurs later after implantation, and often requires invasive treatment.[13] Furthermore, neointimal hyperplasia is the most common but not the only etiology of stent restenosis. Other causes include neoatherosclerosis (calcified or not) and mechanical obstacles such as stent underexpansion and rupture and multiple layered stents in the areas of stent-in-stent deployment.[6] Therefore, stent assessment, especially with noninvasive imaging methods, remains an important but open challenge.

Intravascular ultrasound (IVUS) and optical coherence tomography are the reference to assess the presence, nature, and volume of intrastent lesions.[24] The main differences between these 2 techniques are a better spatial resolution for optical coherence tomography (10-15 μm vs 100-150 μm for IVUS), coupled with a more restricted penetration depth (limited to 2-3 mm).[25] Very importantly, both techniques are invasive and require the presence of the instruments within the coronary artery. Coronary artery CTA is nowadays the only noninvasive alternative for stent lumen evaluation and the only option for global stent and adjacent tissues assessment.

However, imaging of these small, metallic structures placed on beating coronary arteries remains an ordeal for EID CT systems. Spatial resolution is a key factor because stent strut thickness is in the order of 0.07 to 0.08 mm and the caliber of the stent lumen varies, depending on the dimensions of the target coronary artery, with the smallest options being 2.25 mm. Spectral photon counting CT allows detection of up to 28 line-pairs close to the isocenter corresponding to a line thickness of 178 μm, which, although still larger than the stent struts, constitute a remarkable advance compared with EID and nears the limits of IVUS.[10] Artifacts are the other decisive limitation for stent assessment with CT. Small dense structures, such as the stent metallic struts and the adjacent calcifications, are particularly prone to blooming artifacts, which derive from partial volume averaging of different densities within a single voxel and result in objects looking larger than they are in reality.[26] Thanks in particular to the improved spatial resolution, CT systems with PCDs are expected to show a reduction of these artifacts as demonstrated recently in phantoms and in humans.[10,12,27,28] The first in vitro and animal studies focusing on stent assessment with PCCT also point to the same direction.[15–18]

These studies have shown that the density inside the lumen of the stent is less affected by artifacts with SPCCT, resulting in improved subjective evaluation.[15,17–19] In addition, thanks to the reduction of blooming artifacts, measurements of metallic struts proved to be more comparable with nominal values, with internal diameters being larger and external diameters smaller with SPCCT.[16,18] These ameliorations resulted in better detection and characterization of simulated pathology, such as ISR and stent structure deformation due to the presence of calcifications.[16,17] Our results, the first ever in humans, confirm these findings.

Interestingly, albeit not surprisingly, the higher frequency filter on SPCCT (SPCCT-Sharp), combined with a matrix of 1024 and thin slice thickness of 0.25 mm for an isotropic voxel of 0.25 mm^3, was necessary to highlight the reduction of intrastent blooming artifacts. Previous studies on EID and a recent in vitro study on PCCT have already confirmed that kernels with increased 50% modulation transfer function ($MTF_{50\%}$) such as XCD (and SPCCT-Sharp that has an $MTF_{50\%}$ of 17.5 lp/cm at isocenter vs 15.8 lp/cm for the Detailed 2) are more appropriate to depict stent lumina.[29,30] On the other hand, as expected, higher matrix and $MTF_{50\%}$, as well as smaller slice thickness, resulted in increased noise. Nevertheless, this added noise did not hamper subjective evaluation as it did not prevent the SPCCT-Sharp kernel from scoring higher in stent structure and beam-hardening assessment. However, it should be noticed that for the latter, the subjective scores were near 3, the threshold for good diagnostic value. We hypothesize that this is because of the exacerbation of streaks of beam-hardening by motion.[31]

Indeed, having a detector coverage of only 64 × 0.275 mm, the current SPCCT prototype is not yet optimal to depict the heart, a beating structure of about 10 cm in the z-axis, especially in comparison with other EID CT systems with wider coverage or 2 tubes (or even to the expected improvement of the next commercial SPCCT).[32] In the current study, the patients' heart rate was not only similar for the 2 CT scanners but also rather low (around 60 beats per minute), thus impeding any further reasoning on the high heart frequency effect on SPCCT image quality. Another aspect where one might expect to find a negative impact of the SPCCT limited detectors coverage is radiation dose. In fact, a wider detector coverage, allowing scanning the entire heart in a reduced amount of time or even in a single beat, enables to reduce radiation dose.[33] However, notwithstanding the 64 × 0.275 mm coverage, SPCCT showed improved objective and subjective image quality with a beneficial 32% dose reduction as compared with a commercial EID-DLCT with a more than doubled coverage, both used with the same retrospectively ECG-gated acquisition mode.

The present study has limitations that should be mentioned. The first limitation of this pilot study is the small number of included subjects especially when looking on a per-type of stent basis. This did not allow us to draw more conclusions regarding the differences between stent types. Another essential limitation is constituted by the broad inclusion criteria and lack of other reference imaging methods. As a consequence, further prospective studies will have to ascertain that the improved image quality of SPCCT translates in more accurate ISR detection. Nevertheless, our initial findings did demonstrate that calcifications could be easily distinguished from the stent structure with SPCCT, and other complications, such as struts tearing, could be suspected only on SPCCT, thus encouraging the authors to believe in the reproducibility of the presented results also in patients with ascertained stent pathology. Last but not least, SPCCT being a prototype, some technical limitations still exist that have surely influenced our proceedings and likely added some variability. For instance, although we used an identical injection protocol for the 2 examinations, the timing of the injection had to be calculated in different ways on the 2 scanners. Furthermore, aiming to have matching parameters on the 2 systems and taking into account some technical limitations on SPCCT, we used a retrospectively ECG-gated acquisition and did not implement all the available dose-sparing features routinely used on the EID-DLCT. This explains the apparently high radiation dose values for this commercial scanner as compared with what can be achieved for dose-optimized cardiac examinations with dedicated last-generation CT scanners.

In conclusion, in-human coronary stent imaging with SPCCT angiography yields improved objective and subjective image quality in direct comparison with a commercially available EID-DLCT. Therefore, SPCCT is likely to overcome the current limits of CT for clinical stent assessment, the hardest challenge of coronary CT.

REFERENCES

1. Knuuti J, Wijns W, Saraste A, et al. 2019 ESC guidelines for the diagnosis and management of chronic coronary syndromes. *Eur Heart J.* 2020;41:407–477. doi:10.1093/eurheartj/ehz425.

© 2021 The Author(s). Published by Wolters Kluwer Health, Inc.

2. Collet JP, Thiele H, Barbato E, et al. 2020 ESC guidelines for the management of acute coronary syndromes in patients presenting without persistent ST-segment elevation. *Eur Heart J*. 2021;42:1289–1367. doi:10.1093/eurheartj/ehaa575.
3. Mahnken AH. CT imaging of coronary stents: past, present, and future. *ISRN Cardiol*. 2012;2012:139823. doi:10.5402/2012/139823.
4. Dai T, Wang JR, Hu PF. Diagnostic performance of computed tomography angiography in the detection of coronary artery in-stent restenosis: evidence from an updated meta-analysis. *Eur Radiol*. 2018;28:1373–1382. doi:10.1007/s00330-017-5097-0.
5. de Graaf FR, Schuijf JD, van Velzen JE, et al. Diagnostic accuracy of 320-row multidetector computed tomography coronary angiography to noninvasively assess in-stent restenosis. *Invest Radiol*. 2010;45:331–340. doi:10.1097/RLI.0b013e3181dfa312.
6. Shlofmitz E, Iantorno M, Waksman R. Restenosis of drug-eluting stents. *Circ Cardiovasc Interv*. 2019;12:1–8. doi:10.1161/CIRCINTERVENTIONS.118.007023.
7. Piccolo R, Stefanini GG, Franzone A, et al. Safety and efficacy of resolute zotarolimus-eluting stents compared with everolimus-eluting stents: a meta-analysis. *Circ Cardiovasc Interv*. 2015;8:e002223. doi:10.1161/CIRCINTERVENTIONS.114.002223.
8. Taguchi K, Blevis I, Iniewski K. *Spectral, Photon Counting Computed Tomography*. Boca Raton, FL: CRC Press; 2021.
9. Si-Mohamed S, Bar-Ness D, Sigovan M, et al. Review of an initial experience with an experimental spectral photon-counting computed tomography system. *Nucl Instrum Methods Phys Res Sect A Accel Spectrometers Detect Assoc Equip*. 2017;873:27–35. doi:10.1016/j.nima.2017.04.014.
10. Si-Mohamed S, Boccalini S, Rodesch PA, et al. Feasibility of lung imaging with a large field-of-view spectral photon-counting CT system. *Diagn Interv Imaging*. 2021;102:305–312. doi:10.1016/j.diii.2021.01.001.
11. Boccalini S, Si-Mohamed S, Dessouky R, et al. Feasibility of human vascular imaging of the neck with a large field-of-view spectral photon-counting CT system. *Diagn Interv Imaging*. 2021;102:329–332. doi:10.1016/j.diii.2020.12.004.
12. Symons R, Pourmorteza A, Sandfort V, et al. Feasibility of dose-reduced chest CT with photon-counting detectors: initial results in humans. *Radiology*. 2017;285:980–989. doi:10.1148/radiol.2017162587.
13. Sarno G, Lagerqvist B, Fröbert O, et al. Lower risk of stent thrombosis and restenosis with unrestricted use of 'new-generation' drug-eluting stents: a report from the nationwide Swedish Coronary Angiography and Angioplasty Registry (SCAAR). *Eur Heart J*. 2012;33:606–613. doi:10.1093/eurheartj/ehr479.
14. Si-Mohamed SA, Sigovan M, Hsu JC, et al. In vivo molecular K-edge imaging of atherosclerotic plaque using photon-counting CT. *Radiology*. 2021;300:98–107. doi:10.1148/radiol.2021203968.
15. Symons R, De Bruecker Y, Roosen J, et al. Quarter-millimeter spectral coronary stent imaging with photon-counting CT: initial experience. *J Cardiovasc Comput Tomogr*. 2018;12:509–515. doi:10.1016/j.jcct.2018.10.008.
16. Sigovan M, Si-Mohamed S, Bar-Ness D, et al. Feasibility of improving vascular imaging in the presence of metallic stents using spectral photon counting CT and K-edge imaging. *Sci Rep*. 2019;9:19850. doi:10.1038/s41598-019-56427-6.
17. Bratke G, Hickethier T, Bar-Ness D, et al. Spectral photon-counting computed tomography for coronary stent imaging: evaluation of the potential clinical impact for the delineation of in-stent restenosis. *Invest Radiol*. 2020;55:61–67. doi:10.1097/RLI.0000000000000610.
18. Mannil M, Hickethier T, Von Spiczak J, et al. Photon-counting CT: high-resolution imaging of coronary stents. *Invest Radiol*. 2018;53:143–149. doi:10.1097/RLI.0000000000000420.
19. Petritsch B, Petri N, Weng AM, et al. Photon-counting computed tomography for coronary stent imaging: in vitro evaluation of 28 coronary stents. *Invest Radiol*. 2021;56:653–660. doi:10.1097/rli.0000000000000787.
20. Steadman R, Herrmann C, Livne A. Nuclear instruments and methods in physics research a ChromAIX2: a large area, high count-rate energy-resolving photon counting ASIC for a spectral CT prototype. *Nucl Inst Methods Phys Res A*. 2017;862:18–24. doi:10.1016/j.nima.2017.05.010.
21. Boccalini S, den Harder AM, Witsenburg M, et al. Computed tomography image quality of aortic stents in patients with aortic coarctation: a multicentre evaluation. *Eur Radiol Exp*. 2018;2:17. doi:10.1186/s41747-018-0046-5.
22. Stefanini GG, Holmes DR Jr. Drug-eluting coronary-artery stents. *N Engl J Med*. 2013;368:254–265. doi:10.1056/NEJMra1210816.
23. Maron DJ, Hochman JS, Reynolds HR, et al. Initial invasive or conservative strategy for stable coronary disease. *N Engl J Med*. 2020;382:1395–1407. doi:10.1056/NEJMoa1915922.
24. Mehran R, Mintz GS, Hong MK, et al. Validation of the in vivo intravascular ultrasound measurement of in-stent neointimal hyperplasia volumes. *J Am Coll Cardiol*. 1998;32:794–799. doi:10.1016/S0735-1097(98)00316-7.
25. Waksman R, Kitabata H, Prati F, et al. Intravascular ultrasound versus optical coherence tomography guidance. *J Am Coll Cardiol*. 2013;62(suppl 17):S32–S40. doi:10.1016/j.jacc.2013.08.709.
26. Pugliese F, Cademartiri F, van Mieghem C, et al. Multidetector CT for visualization of coronary stents. *Radiographics*. 2006;26:887–904. doi:10.1148/rg.263055182.
27. Si-mohamed SA, Greffier J, Miailhes J, et al. Comparison of image quality between spectral photon-counting CT and dual-layer CT for the evaluation of lung nodules: a phantom study [published online ahead of print June 29, 2021]. *Eur Radiol*.
28. van der Werf NR, Si-Mohamed S, Rodesch PA, et al. Coronary calcium scoring potential of large field-of-view spectral photon-counting CT: a phantom study [published online ahead of print July 13, 2021]. *Eur Radiol*.
29. Tan S, Soulez G, Diez Martinez P, et al. Coronary stent artifact reduction with an edge-enhancing reconstruction kernel—a prospective cross-sectional study with 256-slice CT. *PLoS One*. 2016;11:e0154292. doi:10.1371/journal.pone.0154292.
30. Von Spiczak J, Mannil M, Peters B, et al. Photon counting computed tomography with dedicated sharp convolution kernels: tapping the potential of a new technology for stent imaging. *Invest Radiol*. 2018;53:486–494. doi:10.1097/RLI.0000000000000485.
31. Barrett JF, Keat N. Artifacts in CT: recognition and avoidance. *Radiographics*. 2004;24:1679–1691. doi:10.1148/rg.246045065.
32. Lin E, Alessio A. What are the basic concepts of temporal, contrast, and spatial resolution in cardiac CT? *J Cardiovasc Comput Tomogr*. 2009;3:403–408. doi:10.1016/j.jcct.2009.07.003.
33. Litmanovich DE, Tack DM, Shahrzad M, et al. Dose reduction in cardiothoracic CT: review of currently available methods. *Radiographics*. 2014;34:1469–1489. doi:10.1148/rg.346140084.

© 2021 The Author(s). Published by Wolters Kluwer Health, Inc.